Utilizing dynamic laser speckle to probe nanoscale morphology evolution in nanoporous gold thin films

Christopher A. R. Chapman,[1] Sonny Ly,[2] Ling Wang,[3] Erkin Seker,[3] and Manyalibo J. Matthews[2,*]

[1]*Department of Biomedical Engineering, University of California – Davis, Davis, CA 95616, USA*
[2]*Lawrence Livermore National Laboratory, Livermore, CA 94550, USA*
[3]*Department of Electrical Engineering, University of California – Davis, Davis, CA 95616, USA*
**ibo@llnl.gov*

Abstract: This paper demonstrates the use of dynamic laser speckle autocorrelation spectroscopy in conjunction with the photothermal treatment of nanoporous gold (np-Au) thin films to probe nanoscale morphology changes during the photothermal treatment. Utilizing this spectroscopy method, backscattered speckle from the incident laser is tracked during photothermal treatment and both the characteristic feature size and annealing time of the film are determined. These results demonstrate that this method can successfully be used to monitor laser-based surface modification processes without the use of *ex-situ* characterization.

OCIS codes: (350.3390) Laser materials processing; (310.6628) Subwavelength structures, nanostructures; (290.5880) Scattering, rough surfaces; (300.6480) Spectroscopy, speckle; (150.5495) Process monitoring and control; (240.6648) Surface dynamics.

References and links

1. S. Kirsch, V. Frenz, W. Schartl, E. Bartsch, and H. Sillescu, "Multispeckle autocorrelation spectroscopy and its application to the investigation of ultraslow dynamical processes," J. Chem. Phys. **104**(4), 1758–1761 (1996).
2. M. Erpelding, A. Amon, and J. Crassous, "Diffusive wave spectroscopy applied to the spatially resolved deformation of a solid," Phys. Rev. E Stat. Nonlin. Soft Matter Phys. **78**(4), 046104 (2008).
3. V. Viansoff and F. Lequeux, "Multispeckle diffusing-wave spectroscopy: A tool to study slow relaxation and time-dependent dynamics," Rev. Sci. Instrum. **73**(6), 2336–2344 (2002).
4. L. Schade, S. Franzka, S. Hardt, H. Wiggers, and N. Hartmann, "Sintering of thin titanium dioxide nanoparticle films via photothermal processing with ultraviolet continuous-wave lasers," Appl. Surf. Sci. **278**, 336–340 (2013).
5. D. R. Austin, K. R. Kafka, S. Trendafilov, G. Shvets, H. Li, A. Y. Yi, U. B. Szafruga, Z. Wang, Y. H. Lai, C. I. Blaga, L. F. DiMauro, and E. A. Chowdhury, "Laser induced periodic surface structure formation in germanium by strong field mid IR laser solid interaction at oblique incidence," Opt. Express **23**(15), 19522–19534 (2015).
6. L. E. Murr, S. M. Gaytan, D. A. Ramirez, E. Martinez, J. Hernandez, K. N. Amato, P. W. Shindo, F. R. Medina, and R. B. Wicker, "Metal fabrication by additive manufacturing using laser and electron beam melting technologies," J. Mater. Sci. Technol. **28**(1), 1–14 (2012).
7. M. Mathieu and N. Hartmann, "Sub-wavelength patterning of organic monolayers via nonlinear processing with continuous-wave lasers," New J. Phys. **12**(12), 125017 (2010).
8. A. Lehmann, C. Bradac, and R. P. Mildren, "Two-photon polarization-selective etching of emergent nano-structures on diamond surfaces," Nat. Commun. **5**, 3341–3347 (2014).
9. M. J. Matthews, S. T. Yang, N. Shen, S. Elhadj, R. N. Raman, G. Guss, I. L. Bass, M. Nostrand, and P. J. Wegner, "Micro-Shaping, Polishing, and Damage Repair of Fused Silica Surface Using Focused Infrared Laser Beams," Adv. Eng. Mater. **17**(3), 247–252 (2015).
10. N. Shen, M. J. Matthews, J. E. Fair, J. A. Britten, H. T. Nguyen, D. Cooke, S. Elhadj, and S. T. Yang, "Laser smoothing of sub-micron grooves in hydroxyl-rich fused silica," Appl. Surf. Sci. **256**(12), 4031–4037 (2010).
11. E. Seker, M. L. Reed, and M. R. Begley, "Nanoporous gold: fabrication, characterization, and applications," Materials (Basel) **2**(4), 2188–2215 (2009).
12. K. Li, J. Huang, G. Shi, W. Zhang, and L. Jin, "A sensitive nanoporous gold-based electrochemical DNA biosensor for *Escherichia coli* detection," Anal. Lett. **44**(16), 2559–2570 (2011).

#257075 Received 12 Jan 2016; revised 22 Feb 2016; accepted 24 Feb 2016; published 2 Mar 2016

13. T. Fujita, P. Guan, K. McKenna, X. Lang, A. Hirata, L. Zhang, T. Tokunaga, S. Arai, Y. Yamamoto, N. Tanaka, Y. Ishikawa, N. Asao, Y. Yamamoto, J. Erlebacher, and M. Chen, "Atomic origins of the high catalytic activity of nanoporous gold," Nat. Mater. **11**(9), 775–780 (2012).
14. O. Kurtulus, P. Daggumati, and E. Seker, "Molecular release from patterned nanoporous gold thin films," Nanoscale **6**(12), 7062–7071 (2014).
15. C. A. R. Chapman, H. Chen, M. Stamou, J. Biener, M. M. Biener, P. J. Lein, and E. Seker, "Nanoporous gold as a neural interface coating: effects of topography, surface chemistry, and feature size," ACS Appl. Mater. Interfaces **7**(13), 7093–7100 (2015).
16. M. Li, Y. Du, F. Zhao, J. Zeng, C. Mohan, and W. C. Shih, "Reagent- and separation-free measurements of urine creatinine concentration using stamping surface enhanced Raman scattering (S-SERS)," Biomed. Opt. Express **6**(3), 849–858 (2015).
17. P. Daggumati, Z. Matharu, L. Wang, and E. Seker, "Biofouling-resilient nanoporous gold electrodes for DNA sensing," Anal. Chem. **87**(17), 8618–8622 (2015).
18. M. Hakamada and M. Mabuchi, "Thermal coarsening of nanoporous gold: melting or recrystallization," J. Mater. Res. **24**(02), 301–304 (2009).
19. L. Schade, S. Franzka, M. Mathieu, M. M. Biener, J. Biener, and N. Hartmann, "Photothermal laser microsintering of nanoporous gold," Langmuir **30**(24), 7190–7197 (2014).
20. M. M. Arnob, F. Zhao, J. Zeng, G. M. Santos, M. Li, and W. C. Shih, "Laser rapid thermal annealing enables tunable plasmonics in nanoporous gold nanoparticles," Nanoscale **6**(21), 12470–12475 (2014).
21. P. K. Jain, K. S. Lee, I. H. El-Sayed, and M. A. El-Sayed, "Calculated absorption and scattering properties of gold nanoparticles of different size, shape, and composition: applications in biological imaging and biomedicine," J. Phys. Chem. B **110**(14), 7238–7248 (2006).
22. C. A. R. Chapman, L. Wang, J. Biener, E. Seker, M. M. Biener, and M. J. Matthews, "Engineering on-chip nanoporous gold material libraries via precision photothermal treatment," Nanoscale **8**(2), 785–795 (2016).
23. M. Gale, E. Hogert, N. Gaggioli, H. Rabal, and A. Tavares da Costa, Jr., *Dynamic Laser Speckle and Applications: Chapter 3 - Speckle and Dynamic Speckle Phenomena* (2009).
24. H. Göbel and P. von Blankenhagen, "A study of surface diffusion on gold with an atomic force microscope," Surf. Sci. **331-333**, 885–890 (1995).
25. J. Zeng, F. Zhao, M. Li, C. Li, T. R. Lee, and W. Shih, "Morphological control and plasmonic tuning of nanoporous gold disks by surface modifications," J. Mater. Chem. C Mater. Opt. Electron. Devices **3**(2), 247–252 (2015).

1. Introduction

For many decades, laser speckle autocorrelation spectroscopy has continually demonstrated its utility in determining particle size in colloid suspensions as well as characterizing static material surface properties (i.e. roughness) and slow material relaxation processes [1–3]. The use of speckle patterns to determine these properties presents an attractive avenue for the precise characterization of surfaces during laser materials processing using the existing sources of energy. However, the historically quasi-static nature of this technique (i.e. the measurement of light scattering from objects fixed or slowly varying in space) is not amenable to integration with the wide array of the fast dynamics of laser microprocessing platforms that have seen a rise in recent years for a myriad of applications ranging from direct laser cutting/machining, ablating, additive manufacturing processes, as well as laser-induced periodic surface structure formation (LIPSS) [4–8].

In order to successfully integrate speckle autocorrelation spectroscopy into applications of laser surface processing [9,10], it is necessary to investigate the two-dimensional dynamic laser speckle that arises due to laser-induced surface modification. Specifically, using laser-based methods for the processing of nanostructured materials (metals and polymers) has seen increasing interest in recent years due to the potential for nanostructured materials to improve performance in applications spanning many disciplines ranging from biology to surface catalysis.

Nanostructured materials present a unique albeit challenging surface to characterize via dynamic speckle autocorrelation spectroscopy. One such nanostructured material that lends itself well to surface morphology modification through laser processing is nanoporous gold. Nanoporous gold (np-Au) is a porous metal produced through an alloy corrosion process, known as dealloying, that removes a less noble metal and leaves a three dimensional porous network of nanoscale Au ligaments and pores. Recently np-Au has received attention for its uses in biosensors, neural interfaces, catalysis, tunable molecular release, and the ease of

#257075 Received 12 Jan 2016; revised 22 Feb 2016; accepted 24 Feb 2016; published 2 Mar 2016

morphology modification via photothermal treatment [11–17]. Through the thermal treatment of np-Au it is possible to selectively evolve the Au network thereby altering the characteristic morphology [18], an attractive feature for many emerging np-Au applications. Specifically, photothermal treatment has received attention in order to selectively and precisely modify the np-Au nanostructure [19,20]. Here we couple dynamic laser speckle autocorrelation spectroscopy and the photothermal treatment of thin film np-Au to successfully probe both morphology evolution dynamics (length and time) of the films without the use of *ex situ* microscopy techniques.

2. Materials and methods

2.1 Sample fabrication and characterization

Gold-silver alloy thin films were deposited onto a piranha-cleaned bare or lithographically-patterned silicon wafer. Gold-silver alloy films (precursor to np-Au) were deposited by direct current sputtering (Kurt. J. Lesker). A 600 nm-thick gold and silver alloy film (64% silver and 36% gold; atomic %) was deposited on top of 80 nm-thick gold corrosion barrier and 50 nm-thick chromium adhesion layer. The np-Au films were obtained by immersing the gold-silver alloy in heated (55°C) nitric acid (70%) for 15 minutes. The short dealloying times used in the present study typically result in residual silver levels in the order of 3-5%. The samples were then soaked in deionized (DI) water for 24 hours before drying under nitrogen flow. The morphology of the coatings was characterized by scanning electron microscopy (FEI Nova NanoSEM430), and elemental compositions before and after dealloying were assessed with energy dispersive X-ray spectroscopy (Oxford INCA, Energy-EDS).

2.2 Photothermal treatment of np-Au films

Laser-based photothermal treatment was carried out using a set-up with continuous-wave (CW) laser as the processing laser (Fig. 1). In this set-up a CW laser (SproutD, Lighthouse Photonics) operating at a wavelength of $\lambda = 532$ nm was focused to a 15 μm $1/e^2$ Gaussian spot onto the sample through a 5X/0.14NA objective (Mitutoyo M Plan Apo). A wavelength of 532 nm was chosen for the photothermal treatment of the np-Au film due to the high absorption and scattering rate of gold in the green range [21]. Samples were mounted on a motorized XY stage (ASI MS2000) with manual Z axis control for focus. The sample surface and laser diameter were continually monitored during the experiments using a CCD camera (Basler A102f). Stage, laser, shutter, and camera control was accomplished through a custom LabVIEW control program that enables the complete automation of the laser processing.

2.3 Speckle acquisition and analysis

The far-field backscattered speckle pattern during laser processing was collected to a mounted high frame-rate CMOS camera (Mikrotron EoSens MC1362) using a 20X/0.28NA objective (Mitutoyo M Plan Apo) focused onto the laser spot from an approximate 45° angle. The speckle pattern evolution during annealing was imaged at 939 frames per second and saved as an image sequence using the previously mentioned LabVIEW control program. All subsequent analysis (autocorrelation and curve fitting) was performed using a custom MATLAB program following the equations presented in this manuscript.

2.4 Finite element modeling

The supporting information of our previous manuscript [22] contains detailed parameters regarding the finite element modeling done in this manuscript. All parameters used in this manuscript were held constant except that a laser spot size of 15 μm was used in all simulations here.

#257075 Received 12 Jan 2016; revised 22 Feb 2016; accepted 24 Feb 2016; published 2 Mar 2016

3. Results and discussion

The photothermal treatment and subsequent morphology changes of many porous metals have been demonstrated previously [19,22]. Nanoporous gold (np-Au) presents a good model material for the characterization of surface morphology changes due to an almost ten-fold increase in pore area over a wide range of laser powers [22]. Adding a high frame-rate CMOS camera to an existing CW laser annealing set-up used for the processing of np-Au thin films (Fig. 1) it is possible to accurately and quickly capture the dynamic backscattered speckle pattern from the changing nanostructured surface.

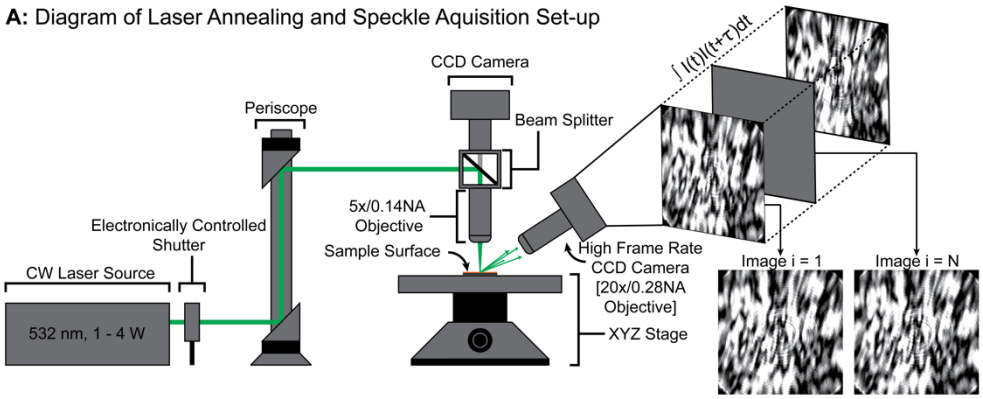

Fig. 1. Laser annealing set-up used to both photothermally anneal and capture backscattered speckle pattern from the changing surface morphology of thin film np-Au.

3.1 Photothermal treatment and morphological characterization

For these experiments, np-Au films were fabricated on silicon substrates. The np-Au films were characterized to have an average ligament width of 30.34 ± 1.26 nm (Fig. 2).

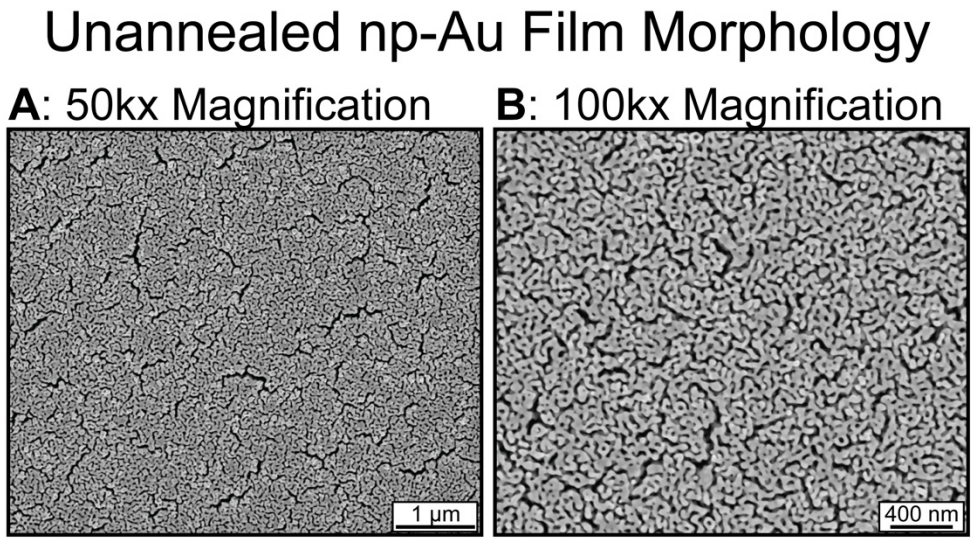

Fig. 2. Scanning electron micrographs of the np-Au film morphology before being photothermally treated: (A) 50kx, (B) 100kx

#257075 Received 12 Jan 2016; revised 22 Feb 2016; accepted 24 Feb 2016; published 2 Mar 2016

A wide range of laser powers were then used to anneal the np-Au films ranging from 1 to 3 W (power at the laser source) in 250 mW increments. Each individual power was exposed to the np-Au surface for 1065 milliseconds with no stage movement. The resulting morphology after photothermal treatment at each power was then captured through scanning electron microscopy. Scanning electron micrographs of the nanostructural changes resulting from laser powers below 2.25 W are shown below (Fig. 3). Laser powers above 2.25 W are not shown here, or analyzed, due to ablation of the film during the laser exposure.

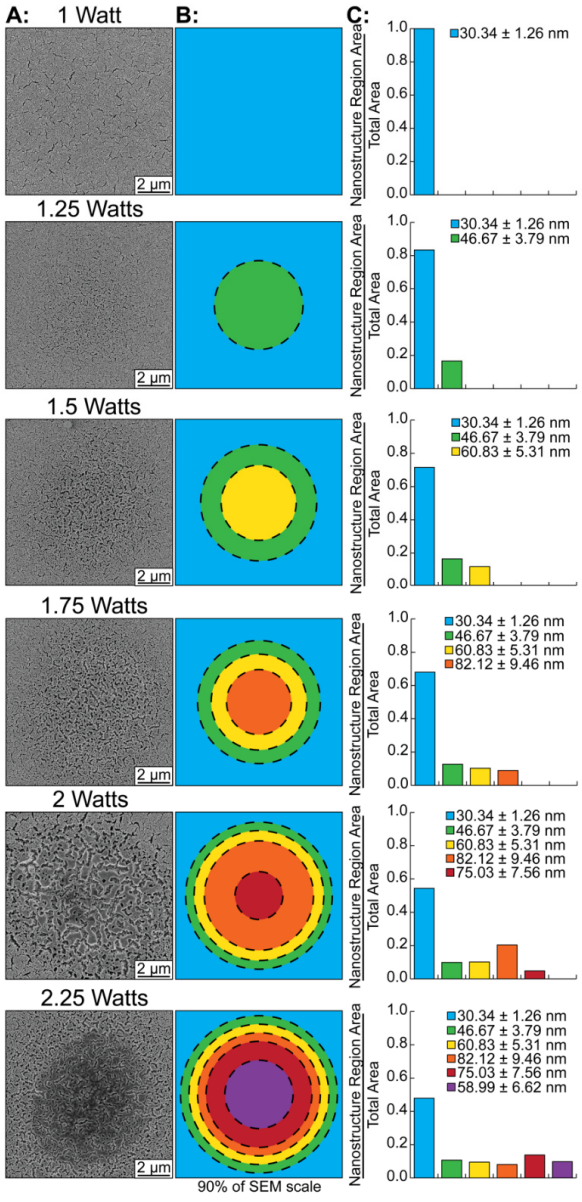

Fig. 3. (A) Scanning electron microscopy images of the nanostructural changes in the np-Au film resulting from laser irradiation at increasing powers. (B) Tracking and differentiation of nanostructure regimes that arise in the np-Au coarsening. (C) Quantification of average ligament width and area fraction (as seen by a 15 μm diameter laser spot) of each nanostructure regime of coarsening.

#257075 Received 12 Jan 2016; revised 22 Feb 2016; accepted 24 Feb 2016; published 2 Mar 2016

The scanning electron micrographs shown in Fig. 3 clearly demonstrate the significant nanostructural changes that occur solely due to increases in power of the working laser. Using custom MATLAB and ImageJ macros each image was split into regions of annealing that corresponded to an overall shift in average feature size. The boundaries of each region were identified visually by the dramatic changes in np-Au morphology. The area contribution of these regions were then calculated and plotted to illustrate the shifting overall feature size of the working area. At a laser power of 1 W no difference in the feature size is seen. At powers between 1.25 W and 2 W there is an increase in feature size as each new region appears. However, at 2 W and 2.25 W, new regions with diminishing feature sizes appear that present morphologies consistent with the beginnings of film ablation that is seen in the higher powers. These regions appear different in contrast and darkness to the other regions due primarily to differences in the film height caused by the sintering of the np-Au in that location.

3.2 Autocorrelation analysis

During each of these photothermal treatments the scattered speckle pattern was captured at 939 frames per second and sequenced into 1000 individual frames. Autocorrelation of a signal is accomplished through cross-correlation of the beginning signal with itself at a delay time, τ, as pictured in Eq. (1):

$$R(\tau) = \int_{-\infty}^{\infty} f(u)\bar{f}(u-\tau)du \tag{1}$$

where $\bar{f}$ is the complex conjugate of the signal function and the integration is over the time delay τ. However, because this method is computationally slow, for a discrete signal it is often more efficient to compute the autocorrelation function through discrete Fourier transforms:

$$\begin{aligned} R(\tau) &= \left\langle IFFT\left\{F_R\left[f(t_o)\right]F_R^*\left[f(t_o+\tau)\right]\right\}\right\rangle \\ F_R\left[f(t_o)\right] &= FFT\left[f(t_o)\right] \end{aligned} \tag{2}$$

where IFFT and FFT represent the inverse fast Fourier transform and the fast Fourier transform respectively. Here we have used the discrete Fourier transform method [Eq. (2)] for the computation of the autocorrelation function from the 1000 frame speckle signal collected from each 1065 millisecond photohermal treatments of the np-Au films.

The dynamic laser speckle from the photothermal treatment at each power tested was collected twice and the autocorrelation function for each was calculated. For clarity purposes the average of the autocorrelation functions was taken for each laser power tested [Fig. 3(a)]. These functions demonstrate clear differences between the behaviors of the dynamic laser speckle signal collected during photothermal treatment at increasing laser power (i.e. film temperature). The scanning electron microscope images of each laser spot (Fig. 3) and the autocorrelation functions calculated from the scattered dynamic laser speckle [Fig. 4(a)] suggest that both morphology evolution time and characteristic length scale might be derived from this analysis.

3.3 Determining characteristic time and feature size through curve fitting

Traditionally in many static techniques, such as colloidal suspensions, the autocorrelation function is fitted to dynamic models from which static parameters can be obtained, such as Brownian motion. However, many models exist for correlating the speckle autocorrelation function to a physically meaningful dynamic entity such as the change in surface roughness as a function of time. As demonstrated by Gale et al. [23], the determination of the surface roughness using reflected dynamic laser speckle can be performed by expressing the autocorrelation function as a function of optical and morphological parameters [Eq. (3)]:

#257075 Received 12 Jan 2016; revised 22 Feb 2016; accepted 24 Feb 2016; published 2 Mar 2016

$$R(\tau) = e^{\left[-(2kn_o\cos\theta)^2\,\delta\sigma^2\right]} \tag{3}$$

where k is the optical field wave-vector given by $2\pi/\lambda$ (λ being laser wavelength), θ is the angle of incidence of the working laser beam, $n_0 \approx 1$ is the index of refraction of the propagating medium (air), and $\delta\sigma$ is the change in surface roughness. The change in surface roughness can then be calculated as a function of the autocorrelation function through rearranging Eq. (3) as:

$$|\delta\sigma| = \frac{\sqrt{-\ln[R(\tau)]}}{2k} \tag{4}$$

given that the angle of incidence in our experiments was held constant at $\theta = 0°$. The values of the change in surface roughness can then be fitted to a decreasing exponential function of the form:

$$\delta\sigma(t) = \delta\sigma_o\left[1 - e^{\left(-t/\tau_p\right)}\right] \tag{5}$$

where $\delta\sigma_o$ and τ_p are fit parameters corresponding to the characteristic feature size and characteristic time associated with representative surface roughness equation. Here, we have utilized this equation to fit the calculated autocorrelation function data collected for each laser power. This was done through first transforming the calculated autocorrelation function data using Eq. (4) and subsequently fitting that data to Eq. (5) [Fig. 4(b)].

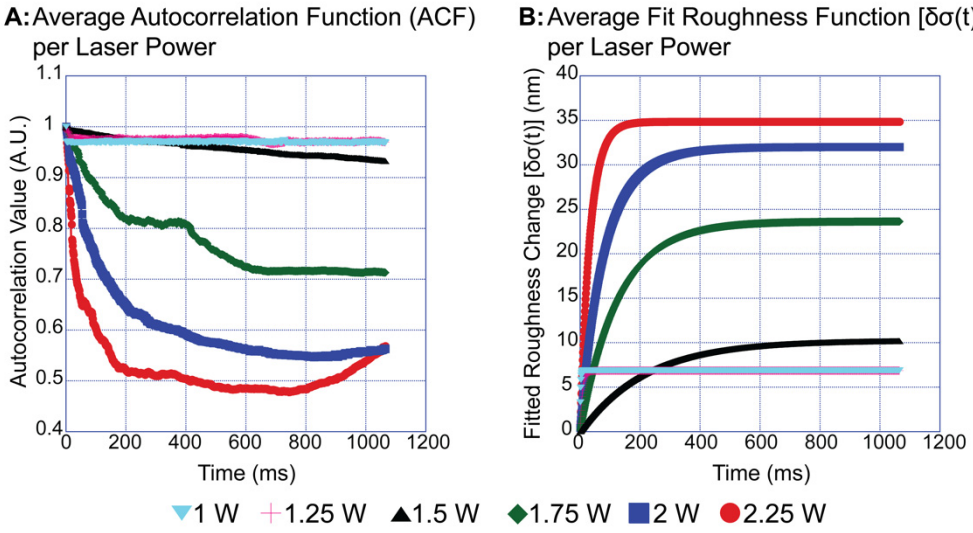

Fig. 4. (A) The averaged autocorrelation function (ACF) as collected from each 1065 second laser spot at varying powers. (B) The averaged surface roughness change derived from a fit of Eq. (5) to each of the autocorrelation functions derived from the average signals seen in (A).

The resulting change in surface roughness functions for each laser power [Fig. 4(b)] demonstrates a clear difference between the behaviors of morphology change during photothermal treatment at laser powers above 1.25 W. Because the 1 W case produced no significant change due to the material nanostructure, the small initial decorrelation in the 1 W case is assumed to be attributed to the thermal expansion of the np-Au film (0.07% at 350 K). Similarly, because the 1.25 W case falls into the same trend, the decorrelation is again primarily attributed to the linear thermal expansion of the film (0.11% at 375 K). To support

#257075 Received 12 Jan 2016; revised 22 Feb 2016; accepted 24 Feb 2016; published 2 Mar 2016

this, we can approximate the decorrelation due to small morphology changes as $R \approx 1-(4\pi/\lambda)^2\delta\sigma^2$, which yields $R \approx 0.99$, in good agreement with the small initial change in R observed in Fig. 4(a) for both 1 W and 1.25 W cases. Although this decorrelation due to linear thermal expansion speaks to the overall sensitivity of this technique, it is not a value that is important for analysis here. However, at laser powers above 1.25 W the decorrelation of the dynamic speckle signal increases as the power of the laser used for photothermal treatment increases. This result is expected due to the morphology evolution of nanoporous gold being highly dependent on the thermal activation of Au surface diffusion. Plotting the fit parameters of characteristic roughness and characteristic time versus laser power used for photothermal treatment a clear trend becomes apparent (Fig. 5). As the laser power increases, the characteristic feature size of fit increases [Fig. 5(a)] and the characteristic time decreases [Fig. 5(b)]. These trends are expected in the temperature dependent annealing of a np-Au film where the diffusion coefficient is directly related to the film temperature. However, whether these fit parameters follow the correct amount of change for the parameters physically observed (change in feature size and change in diffusion time) needs to be validated.

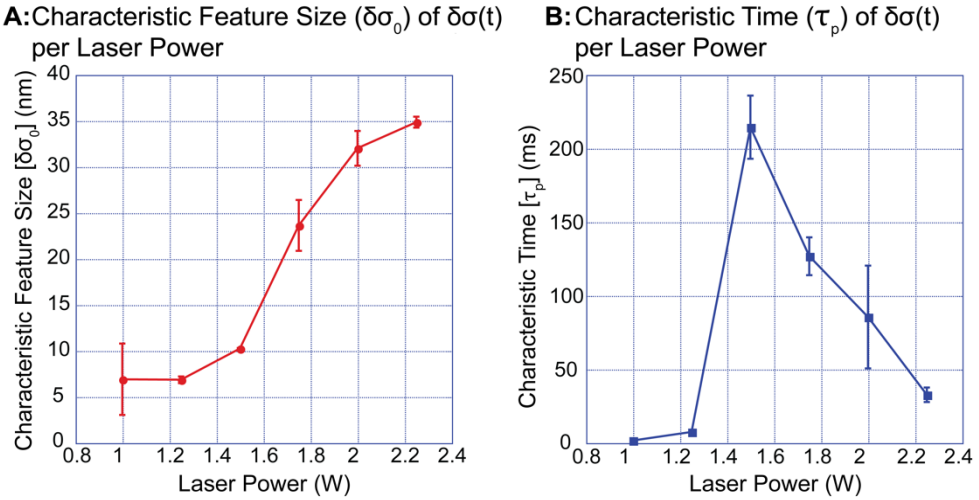

Fig. 5. (A) The characteristic feature size from the fit equation per laser power shows an increase in the surface morphology roughness due to increasing laser power. (B) The characteristic times for the fit roughness equation to reach steady state show a decrease in time with increasing laser power. Laser power of 1 W (no morphology change) and 1.25 W (little morphology change) were above the threshold for detection by this method and therefor both show low characteristic times.

3.4 Validating calculated characteristic feature size and time

The characteristic feature size of each photothermally treated spot, calculated through speckle analysis, increases with the application of increasing laser power, with the exception of 1.25 W [Fig. 5(a)]. In order to validate that the characteristic feature sizes determined through this analysis are correlated to the real nanoscale feature sizes of the film the average feature size of each laser shot (shown in Fig. 3) was calculated by weighing each regions feature size by its area percentage. The resulting feature sizes calculated through dynamic speckle analysis, as well as through image analysis of the spot morphologies calculated by taking a weighted average of the feature sizes using region areas identified in Fig. 3, are shown in Fig. 6(a) where a linear correlation is found with a R^2 value of 0.947 [Fig. 6(b)]. This demonstrates that through using the autocorrelation analysis of the dynamic laser speckle it is possible to correctly estimate the feature size of the film with nanometer sensitivity.

#257075 Received 12 Jan 2016; revised 22 Feb 2016; accepted 24 Feb 2016; published 2 Mar 2016

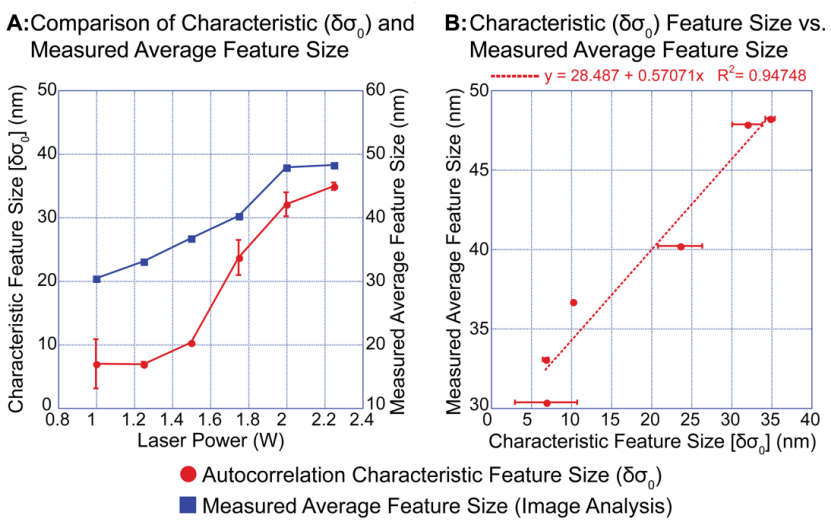

Fig. 6. (A) Characteristic feature sizes calculated from the fitted speckle autocorrelation function (red) and from directly measuring nanostructure via image analysis (blue). (B) The characteristic feature sizes calculated from fitting the calculated speckle autocorrelation function show a strong linear relationship with the feature sizes measured directly via image analysis ($R^2 = 0.947$).

Similarly, the characteristic times calculated through speckle analysis show decreasing time of annealing as laser power is increased [Fig. 5(b)]. This parameter corresponds directly to the time that it took the speckle pattern autocorrelation to reach a steady-state value and therefore is associated with the changing diffusion coefficient in due to laser irradiation. Unfortunately, the time scale used for these experiments was not long enough to capture the characteristic time for powers below 1.5 W. However, disregarding the points above the limit of detection a clear exponential decrease in time versus laser power becomes apparent. In order to validate that the characteristic time calculated through dynamic speckle follows the expected rate of change, we can make a comparison to simulated photothermal heating of a np-Au thin film. Recently, we have shown a simple thermal model for the photothermal annealing of np-Au using a finite element multiphysics program [22].

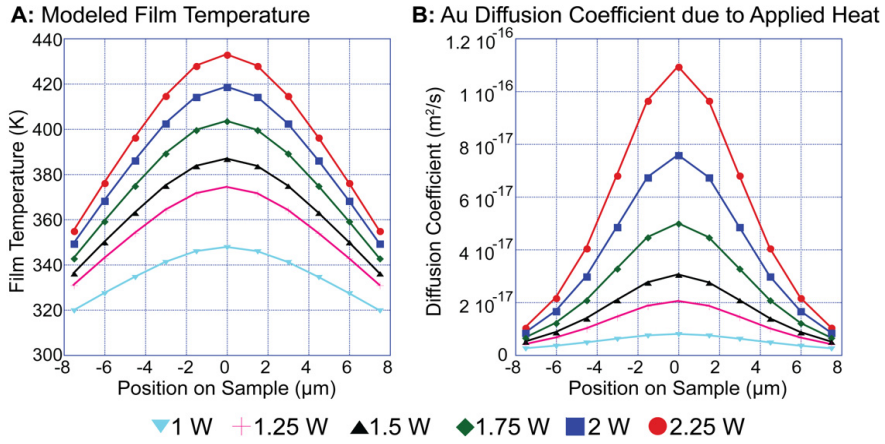

Fig. 7. (A) Distribution of modeled np-Au film temperature caused by irradiation of a 15 μm diameter, λ = 532 nm, laser spot for 1065 seconds. (B) Distribution of the Au diffusion coefficient resulting from the increases in film temperatures modeled.

#257075 Received 12 Jan 2016; revised 22 Feb 2016; accepted 24 Feb 2016; published 2 Mar 2016

Using this model, the Gaussian film temperature of the film can be simulated for each laser power used in this study [Fig. 7(a)], this distribution can then be used to calculate the diffusion coefficient increase due to laser irradiation [Fig. 7(b)] via the Arrhenius relationship for Au surface diffusion [24]. Using the area fractions for each different nanostructure region (shown in Fig. 3) the total diffusion time can be calculated. Plotting the modeled total diffusion time and the calculated characteristic time of the dynamic speckle analysis, without 1 and 1.25 W, shows remarkable similarity between the modeled and calculated times [Fig. 8(a)]. Plotting these values versus the inverse modeled film temperatures seen in Fig. 7, gives exponential factors close to the expected 'ideal' Arrhenius relationship of the activation energy of Au ($\varepsilon_a = 6.41\text{x}10^{-20}$ J) divided by the Boltzmann constant ($k_B = 1.38\text{x}10^{-23}$ J/K), or 4644.92 K [Fig. 8(b)] [24].

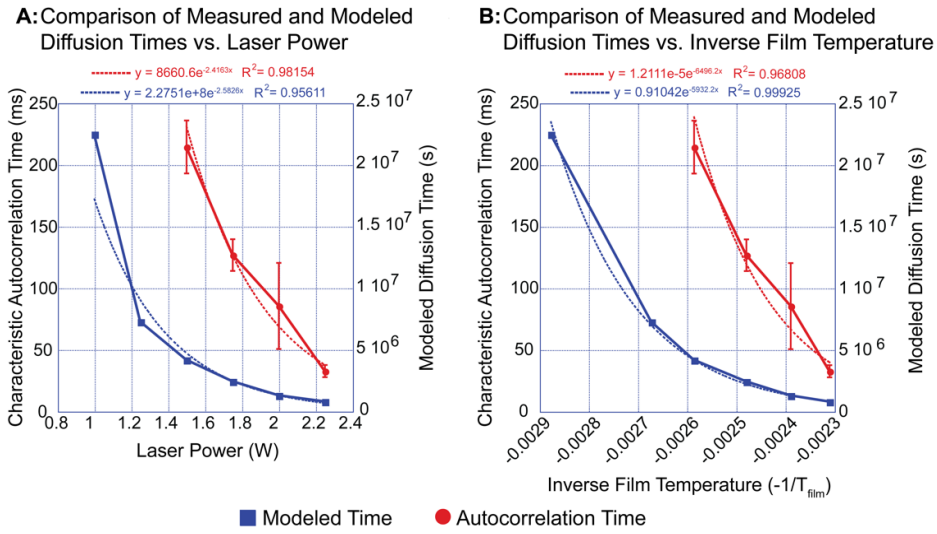

Fig. 8. (A) Characteristic times calculated from the fitted speckle autocorrelation functions (red) and the total diffusion time of the modeled np-Au film (blue) for each laser power used in this study. Both the characteristic time and the modeled diffusion time show strong exponential fits with similar exponential decreases. (B) Plotting these values against inverse film temperature gives exponential factors on the same order of magnitude of the 'ideal' relationship governed by the Arrhenius relationship.

Other optical techniques, such as extinction spectroscopy, have been successfully employed to measure nanostructural changes in np-Au disks [25]. Although the resolution of these processes is high, coupling these processes to existing laser processing techniques to track morphology change *in situ* would prove difficult. Ultimately this method of utilizing dynamic laser speckle to determine the nanostructured morphology change during photothermal treatment shows promise in being directly applied to many laser processing techniques being used in industry and academic research to accurately predict the morphology changes of both microstructured and nanostructured materials being processed *in situ* without the use of external microscopy techniques.

4. Conclusion

In this work we have demonstrated that dynamic laser speckle autocorrelation spectroscopy can be utilized in an *in situ* laser microprocessing environment to probe nanoscale morphology changes of the material being processed. This advancement has the potential to be added into traditional laser materials processing techniques such as ablation, nanoscale coarsening, as well as many metal based additive manufacturing techniques as a feedback control for the system to determine when the material being processed has reached the desired

#257075 Received 12 Jan 2016; revised 22 Feb 2016; accepted 24 Feb 2016; published 2 Mar 2016

change in morphology. Further characterization of the dynamic laser speckle autocorrelation produced from the processing laser with a constant linear velocity is currently underway. By separating the speckle pattern changes due to linear laser beam movement over the sample surface and the thermally-induced morphology change this technique will be applicable as a real time characterization technique for any scanning laser machining process allowing for the simultaneous fabrication and characterization of the material being processed.

Acknowledgments

We gratefully acknowledge the help and support of Gabe Guss regarding both LabVIEW and high-speed camera set-up. Additionally, we acknowledge the support from UC Lab Fees Research Program Award (12-LR-237197) and National Science Foundation Awards (CBET-1512745 and CBET-DMR-1454426). C. Chapman was supported by a National Science Foundation Research Fellowship (DGE-1148897). Any opinion, findings, and conclusions or recommendations expressed in the material are those of the author(s) and do not necessarily reflect the views of the National Science Foundation. Work at LLNL was funded through a Laboratory Directed Research and Development grant (15-ERD-037) and performed under the auspices of the U.S. Department of Energy by Lawrence Livermore National Laboratory under contract DE-AC52-07NA27344.

#257075 Received 12 Jan 2016; revised 22 Feb 2016; accepted 24 Feb 2016; published 2 Mar 2016